Configurational Temperature in Membrane Simulations Using Dissipative Particle Dynamics[†]

Michael P. Allen

Department of Physics and Centre for Scientific Computing, University of Warwick, Coventry CV4 7AL, United Kingdom

Received: September 10, 2005; In Final Form: November 10, 2005

The use of excessively long time steps in dissipative particle dynamics simulations may produce simulation artifacts due to the generation of configurations which are not representative of the desired canonical ensemble. The configurational temperature, among other quantities, may be used to assess the extent of the deviation from equilibrium. This paper presents results for simulations of models of water and lipid bilayer membranes to illustrate the nature of the problems.

1. Introduction

Dissipative particle dynamics[1,2] (DPD) has become a popular tool for simulating the behavior of both simple and complex fluids. In outline, it consists of the solution of the classical equations of motion for a system of interacting particles, together with a set of stochastic and dissipative forces which control the temperature and allow one to choose the viscosity. It is usual to employ a very simple, repulsive, pair potential, often choosing the force law derived from it to vary linearly with separation within a specified cutoff range. As well as these conservative forces, the stochastic and dissipative forces also act in a pairwise fashion, so as to conserve momentum and ensure hydrodynamic behavior. The particles represent fluid regions, rather than individual atoms and molecules: the softness and simplicity of the interactions permit the use of a long time step, compared with conventional molecular dynamics. This, and the acceleration of physical processes compared with those seen in more realistic simulations, gives an advantage of several orders of magnitude, at the cost of a very rough mapping onto specific molecular properties. The way to relate the key DPD parameters to fluid equations of state and transport coefficients has been usefully presented by Groot and Warren.[3]

By tuning the interactions to represent hydrophilic and hydrophobic units, and linking together the particles in a simple bead-spring fashion, the DPD method has been applied to lipid bilayer membranes.[4] Self-assembly and phase diagrams have been investigated,[5] stress profiles determined,[6] and the effects of small molecules[7] and membrane-bound proteins[8] studied.

Several papers have attempted to optimize the computational algorithm used to solve the DPD equations.[9−18] The early emphasis was on the correct handling of the velocity-dependent dissipative forces, and ensuring the correct balance of these with the random forces, at an appropriate time step, so as to generate the canonical ensemble.[19] Accordingly, most attention[3] has focused on maintaining a kinetic temperature T_k (defined in terms of the kinetic energy per degree of freedom, via the equipartition theorem) reasonably close to the desired temperature T. A detailed analysis of the ideal fluid limit,[20] as a function of time step, has been carried out. In addition, it has become standard practice to check the pair distribution function and diffusion coefficient for dependence on the time step, as diagnostic tests.

Recently, increased attention has been paid to the suitability or otherwise of the time step for the integration of the conservative forces. This is particularly important in simulations of multicomponent systems, polymers, and membranes, where some of the interaction potentials may be stronger than others, including intramolecular bond-bending and stretching terms. The usual criterion of molecular dynamics, energy conservation in the absence of random and dissipative forces, is not usually employed, and any problems may be disguised by the thermostating. To generate meaningful results, it is essential to sample configurations from the canonical (Boltzmann) distribution, and any indicator of significant deviations must be taken seriously. den Otter and Clarke[21] were the first to point out that DPD, at the usual time steps and state points, generates configurations for which the *configurational temperature* T_c differs significantly from the desired temperature T and the kinetic temperature T_k. den Otter and Clarke estimated this quantity by calculating (for small time steps) the average potential energy $\langle U\rangle$ as a function of temperature in the vicinity of T and fitting the results to a quadratic curve, then this curve was used to convert averages of $\langle U\rangle$ measured at larger time steps into an estimate of T_c. Here a different, and more straightforward, definition is used. The configurational temperature T_c is written

$$k_B T_c = \frac{\sum_j \langle |\nabla_j U|^2\rangle}{\sum_j \langle \nabla_j^2 U\rangle} \tag{1}$$

where k_B is Boltzmann's constant, ∇_j the gradient, and ∇_j^2 the Laplacian, of the potential energy U, with respect to the position of particle j. The summations may be over all particles in the system or restricted to a single species, or indeed to an individual particle. The expression has long been known as a hypervirial relation.[22,23] It was first introduced by Rugh[24] as an independent estimate of temperature in simulations and recommended as a diagnostic test for lack of equilibrium by Butler et al.[25]

In the context of membrane simulations, Jakobsen et al.[26] observed significant differences in the kinetic temperatures of

[†] Part of the special issue "Michael L. Klein Festschrift".

10.1021/jp055119e CCC: $33.50 © 2006 American Chemical Society
Published on Web 12/23/2005

different species in DPD simulations and recommended this as a simple diagnostic test of incorrect integration of the equations of motion. They also mentioned the possibility of monitoring the configurational temperature but did not report any results for this. However, they observed several other simulation artifacts, including time-step dependence of the pressure profiles and particle densities within the membrane. Hafskjold et al.[27] have reemphasized that the time steps typically recommended and used in DPD are too long to properly handle the discontinuity at the cutoff of the usual conservative force law: they investigated the possibility of softening this cutoff via spline functions, but no dramatic improvements at long time steps were seen, and they recommended the use of shorter time steps.

This paper reports simulation averages of the configurational temperature for a standard single-component DPD fluid, over a range of time steps, using a variety of proposed DPD integration methods. The results show that, although some of these methods dramatically improve the control of the kinetic temperature T_{k}, the same improvements are not seen for the configurational temperature: deviations of T_{c} from the desired values remain significant in all cases, at the typically recommended time steps. Results are then reported for the same membrane model used in ref 26: largely as a result of intramolecular bonding terms in the potential, the deviations in T_{c} are far worse than those in the simple fluid case and may be correlated with some of the other artifacts observed before.[26] The general conclusion is that the configurational temperature should be added to the list of diagnostic tests applied to DPD simulations and that shorter time steps should be employed in membrane simulations than hitherto.

2. Dynamical Algorithms

The DPD equations of motion for a simple fluid may be written[1,2,19]

$$\mathrm{d}\boldsymbol{r}_i = (\boldsymbol{p}_i/m)\,\mathrm{d}t \tag{2a}$$

$$\mathrm{d}\boldsymbol{p}_i = \sum_{j\neq i} \boldsymbol{f}_{ij}{}^{\mathrm{C}}\,\mathrm{d}t + \boldsymbol{f}_{ij}{}^{\mathrm{D}}\,\mathrm{d}t + \mathrm{d}\boldsymbol{p}_{ij}{}^{\mathrm{R}} \tag{2b}$$

The particles are all assumed to have the same mass m. The conservative forces usually take the form

$$\boldsymbol{f}_{ij}^{\mathrm{C}} = \alpha\omega(r_{ij})\hat{\boldsymbol{r}}_{ij} \tag{3a}$$

with

$$\omega(r) = \begin{cases} 1 - r/r_{\mathrm{c}} & r \le r_{\mathrm{c}} \\ 0 & r > r_{\mathrm{c}} \end{cases} \tag{3b}$$

Here $\boldsymbol{r}_{ij} = \boldsymbol{r}_i - \boldsymbol{r}_j$, $r_{\mathrm{ij}} = |\boldsymbol{r}_{ij}|$, $\hat{\boldsymbol{r}}_{ij} = \boldsymbol{r}_{ij}/r_{ij}$. The parameter α determines the strength of the conservative interactions, and r_{c} is the cutoff. The dissipative forces and random impulses are written

$$\boldsymbol{f}_{ij}{}^{\mathrm{D}} = -\gamma\omega(r_{ij})^2(\boldsymbol{v}_{ij}\cdot\hat{\boldsymbol{r}}_{ij})\hat{\boldsymbol{r}}_{ij}$$

$$\mathrm{d}\boldsymbol{p}_{ij}{}^{\mathrm{R}} = \sigma\omega(r_{ij})\hat{\boldsymbol{r}}_{ij}\,\mathrm{d}W_{ij}$$

where $\boldsymbol{v}_{ij} = \boldsymbol{v}_i - \boldsymbol{v}_j$ and $\boldsymbol{p}_i = m\boldsymbol{v}_i$. A choice has been made here to use the same weighting function $\omega(r)$ in the specification of conservative, dissipative, and random terms. The dissipative friction γ is related to the random impulse strength σ by the fluctuation−dissipation theorem $\sigma^2 = 2\gamma k_{\mathrm{B}}T$. The quantity $\mathrm{d}W_{ij}$ is the time derivative of a Wiener process: over a time step Δt, ΔW_{ij} is chosen from a normal distribution with zero mean and variance Δt, and $\Delta W_{ji} = -\Delta W_{ij}$. Units are chosen such that the particle mass m, cutoff r_{c}, and temperature T are all unity.

Four algorithms will be discussed in this paper. The "standard" DPD algorithm consists of the following steps[11,14]

$$\tilde{\boldsymbol{p}}_i := \boldsymbol{p}_i + \lambda \sum_{j\neq i} \boldsymbol{f}_{ij}{}^{\mathrm{C}}\Delta t + \boldsymbol{f}_{ij}{}^{\mathrm{D}}\Delta t + \Delta\boldsymbol{p}_{ij}{}^{\mathrm{R}} \tag{4a}$$

$$\boldsymbol{p}_i := \boldsymbol{p}_i + \frac{1}{2}\sum_{j\neq i} \boldsymbol{f}_{ij}{}^{\mathrm{C}}\Delta t + \boldsymbol{f}_{ij}{}^{\mathrm{D}}\Delta t + \Delta\boldsymbol{p}_{ij}{}^{\mathrm{R}} \tag{4b}$$

$$\boldsymbol{r}_i := \boldsymbol{r}_i + (\boldsymbol{p}_i/m)\Delta t \tag{4c}$$

$$\text{Calculate } \boldsymbol{f}_{ij}{}^{\mathrm{C}}(\{\boldsymbol{r}_i\}),\ \boldsymbol{f}_{ij}{}^{\mathrm{D}}(\{\boldsymbol{r}_i\},\{\tilde{\boldsymbol{p}}_i\}),\ \Delta\boldsymbol{p}_{ij}{}^{\mathrm{R}}(\{\boldsymbol{r}_i\}) \tag{4d}$$

$$\boldsymbol{p}_i := \boldsymbol{p}_i + \frac{1}{2}\sum_{j\neq i} \boldsymbol{f}_{ij}{}^{\mathrm{C}}\Delta t + \boldsymbol{f}_{ij}{}^{\mathrm{D}}\Delta t + \Delta\boldsymbol{p}_{ij}{}^{\mathrm{R}} \tag{4e}$$

$$\text{Calculate } \boldsymbol{f}_{ij}{}^{\mathrm{D}}(\{\boldsymbol{r}_i\},\ \{\boldsymbol{p}_i\}) \tag{4f}$$

Note the auxiliary momenta $\tilde{\boldsymbol{p}}_i$, used in the calculation of dissipative forces, and predicted using a parameter λ. The value $\lambda = 0.5$ conveniently makes $\tilde{\boldsymbol{p}}_i = \boldsymbol{p}_i$, but $\lambda = 0.65$ was found by Groot and Warren[3] to be optimal for the particular fluid that will be studied here. This paper will use $\lambda = 0.65$. Note also the second computation of dissipative forces (step 4f) introduced by Gibson et al.[11] Iteration of the last two steps would lead to a self-consistent algorithm[12] not studied here.

The second algorithm is the so-called "Scheme II" of Peters.[17] At each time step, the positions and momenta are updated using the conservative forces only

$$\boldsymbol{p}_i := \boldsymbol{p}_i + \frac{1}{2}\sum_{j\neq i} \boldsymbol{f}_{ij}{}^{\mathrm{C}}\Delta t \tag{5a}$$

$$\boldsymbol{r}_i := \boldsymbol{r}_i + (\boldsymbol{p}_i/m)\Delta t \tag{5b}$$

$$\text{Calculate } \boldsymbol{f}_{ij}{}^{\mathrm{C}}(\{\boldsymbol{r}_i\}) \tag{5c}$$

$$\boldsymbol{p}_i := \boldsymbol{p}_i + \frac{1}{2}\sum_{j\neq i} \boldsymbol{f}_{ij}{}^{\mathrm{C}}\Delta t \tag{5d}$$

Following this, for every pair i, j, selected in random order, the following update is performed

$$p_i := \boldsymbol{p}_i + \boldsymbol{f}_{ij}{}^{\mathrm{D}}\Delta t + \Delta\boldsymbol{p}_{ij}{}^{\mathrm{R}}$$

$$\boldsymbol{p}_{\mathrm{j}} := \boldsymbol{p}_j - \boldsymbol{f}_{ij}{}^{\mathrm{D}}\Delta t - \Delta\boldsymbol{p}_{ij}{}^{\mathrm{R}}$$

with

$$\boldsymbol{f}_{ij}{}^{\mathrm{D}} = -a_{ij}(v_{ij}\cdot\hat{\boldsymbol{r}}_{ij})\hat{\boldsymbol{r}}_{ij}$$

and

$$\Delta\boldsymbol{p}_{ij}{}^{\mathrm{R}} = b_{ij}\Delta W_{ij}\hat{\boldsymbol{r}}_{ij}$$

The parameters a_{ij} and b_{ij} are determined by T and γ (or, equivalently, T and σ) and by the time step. As explained by Peters,[17] this generates the Maxwell−Boltzmann distribution of velocities and, at short time step, solves the original DPD equations.

The third algorithm is due to Lowe.[10] This is not a solution of the original DPD equations but rather a pairwise thermostat applied to a conventional integration algorithm for the conservative forces. As for the Peters method, at each step the positions and momenta are updated using steps 5a−5d above, using the conservative forces only. Then, by examination of every pair (in random order), with probability $P = \Gamma\Delta t$, the momenta are updated as follows

$$p_i := \boldsymbol{p}_i + \Delta \boldsymbol{p}_{ij}^{\mathrm{R}}$$

$$p_j := \boldsymbol{p}_j - \Delta \boldsymbol{p}_{ij}^{\mathrm{R}}$$

with

$$\Delta \boldsymbol{p}_{ij}^{\mathrm{R}} = \frac{1}{2} m[\zeta\sqrt{2k_{\mathrm{B}}T/m} - (\boldsymbol{v}_{ij}\cdot\hat{\boldsymbol{r}}_{ij})]\hat{\boldsymbol{r}}_{ij}$$

where ζ is selected from a Gaussian distribution with zero mean and unit variance. This procedure reselects the relative velocity from the Maxwell−Boltzmann distribution. The key parameter is the stochastic randomization frequency Γ.

The fourth algorithm to be considered here has been proposed by Stoyanov and Groot.[18] It is identical with the method of Lowe, except that the fraction $(1 - P)$ of pairs which do not have their relative velocities stochastically reselected are instead thermalized by a deterministic method. For each such pair, after steps 5a and 5b, a dissipative force is calculated

$$\boldsymbol{f}_{ij}^{\mathrm{D}} = k\omega(r_{ij})(\boldsymbol{v}_{ij}\cdot\hat{\boldsymbol{r}}_{ij})\hat{\boldsymbol{r}}_{\boldsymbol{ij}}$$

$$\boldsymbol{f}_i^{\mathrm{D}} := \boldsymbol{f}_i^{\mathrm{D}} + \boldsymbol{f}_{ij}^{\mathrm{D}}$$

$$\boldsymbol{f}_j^{\mathrm{D}} := \boldsymbol{f}_j^{\mathrm{D}} - \boldsymbol{f}_{ij}^{\mathrm{D}}$$

Then, after steps 5c and 5d, the momenta are corrected by

$$p_i := \boldsymbol{p}_i + \Delta t(1 - \tilde{T}_k/T)\boldsymbol{f}_i^{\mathrm{D}}$$

where $\tilde{T}_{\mathrm{k}}$ is a kinetic temperature estimated from relative velocities at the start of the time step. Finally, the Lowe velocity reselection process is applied to the remaining fraction P of pairs as usual. In the present work, following ref 18, the parameter k is set to $k = 0.3/\Delta t$. As for the Lowe method, the key parameter is the stochastic randomization rate Γ which determines P. Stoyanov and Groot[18] associate the deterministic part of their thermostat with the Nosé−Hoover algorithm,[28,29] but in practice it seems to be more closely related to that of Berendsen,[30] since the “friction coefficient” is not a dynamical variable but is instead directly proportional to the temperature factor $(1 - \tilde{T}_{\mathrm{k}}/T)$. This approach permits a high degree of temperature control at low, or even zero, values of Γ, where the Lowe method is ineffective: indeed, Stoyanov and Groot report an order of magnitude improvement in T_{k}. However, the links with a statistical ensemble, and with the DPD equations themselves, remain to be established.

3. Simulation Models and Parameters

By considering the equation of state and dynamical properties of water under ambient conditions, Groot and Warren[3] established the standard parameter set that is commonly used in algorithm tests:[14−18] strength parameter $\alpha = 25$, number density $\rho = 3$, stochastic impulse strength $\sigma = 3$, and hence (for $T = 1$) $\gamma = 4.5$. This is sometimes referred to as “Model B”. This paper reports results for Model B, and also for variants with $\sigma = 1$ and $\sigma = 6$, using both the DPD and Peters methods. For the Stoyanov−Groot and Lowe algorithms, stochastic collision rates $\Gamma = 0$, 0.2, 4, and the maximum possible $\Gamma = 1/\Delta t$ (corresponding to $P = 1$, completely reselecting all velocities every time step) are investigated. A system size of $N = 250$ particles in a cubic box with periodic boundary conditions is used throughout.

For their tests of DPD simulations of membranes, Jakobsen et al.[26] adopted the model of Shillcock and Lipowsky.[6] Each lipid molecule has the form of a seven-bead chain HT_6 in which repulsion parameters between hydrophilic “head” beads (H), hydrophobic “tail” beads (T), and “water” beads (W) are as follows: $\alpha_{\mathrm{WW}} = \alpha_{\mathrm{HH}} = \alpha_{\mathrm{TT}} = 25$, $\alpha_{\mathrm{HW}} = 35$, $\alpha_{\mathrm{HT}} = 50$, $\alpha_{\mathrm{TW}} = 75$. Successive lipid beads are connected by harmonic springs, and a simple bond-bending potential favors linearity

$$u_{\mathrm{stretch}}(\boldsymbol{r}_{ij}) = \frac{1}{2} k_{\mathrm{stretch}}(r_{ij} - l_0)^2 \tag{6a}$$

with $k_{\mathrm{stretch}} = 128, \quad l_0 = 0.5$

$$u_{\mathrm{bend}}(\boldsymbol{r}_{ij}, \boldsymbol{r}_{jk}) = k_{\mathrm{bend}}(1 - \hat{\boldsymbol{r}}_{ij}\cdot\hat{\boldsymbol{r}}_{jk}) \tag{6b}$$

with $k_{\mathrm{bend}} = 20$

The present paper uses this model but follows Jakobsen et al.[26] in choosing all stochastic impulse strengths to be the same, $\sigma = 3$, in the DPD and Peters algorithms. For comparison, results obtained using the Stoyanov−Groot method with $\Gamma = 0$ and using the Lowe thermostat with $\Gamma = 1/\Delta t$ are reported. A smaller system is used here than in the previous papers:[6,26] $N_{\mathrm{lipid}} = 100$ lipid chains plus $N_{\mathrm{water}} = 2500$ water beads, making $N = 3200$ beads in all. A cuboidal box, with periodic boundaries, was employed. Transverse box dimensions were fixed so as to give an overall number density $\rho = 3$, and an area per lipid $2A/N_{\mathrm{lipid}} = 0.617$, close to the state of zero surface tension. The chains were preformed into a flat bilayer, and allowed to equilibrate before any measurements were made.

The time unit $\tau = r_{\mathrm{c}}(m/k_{\mathrm{B}}T)^{1/2}$ is defined in terms of the other fixed parameters. In these units, for the water model described above, Groot and Warren[3] recommend time steps in the range $\Delta t = 0.04 \ldots 0.06$, so as to achieve an accuracy of order 1% in T_{k}; the present paper investigates time steps in the range $0.005 \le \Delta t \le 0.06$. Total simulation times for the water runs were $t_{\mathrm{run}} = 2000$, and for the membrane runs were $t_{\mathrm{run}} = 10000$. Formulas for the Laplacians used to calculate the configurational temperature for this model are given in the Appendix.

4. Results

Figures 1 and 2 show the measured temperatures for the four chosen algorithms, in simulating the water model at various choices of thermostating strength. With an appropriate choice of parameters, it is indeed possible to achieve a kinetic temperature T_{k} within 1% of the desired value at a time step $\Delta t = 0.05$; the Stoyanov−Groot method performs well in this regard at all values of Γ, and the Lowe thermostat is good at high values of Γ. The more recently developed thermostats all seem less sensitive to variations in σ or Γ than the basic DPD algorithm. However, it can be seen that the error in the configurational temperature T_{c} is an order of magnitude worse than that in T_{k}, being around 10% at $\Delta t = 0.05$, and this is not dramatically affected by the choice of algorithm: the “best” (Stoyanov−Groot at $\Gamma = 0$) reduces the error by 30−40% compared to the “worst” (all of the methods, at high stochastic thermalization rate). Also, for quite small stochastic damping

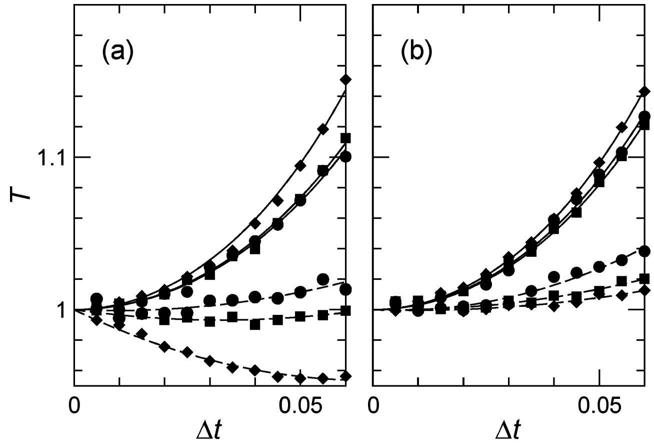

Figure 1. Water simulations using (a) DPD algorithm with $\lambda = 0.65$ and (b) Peters Scheme II: temperatures as functions of time step Δt; solid lines, configurational temperature T_c; dashed lines, kinetic temperature T_k; circles, $\sigma = 1$; squares, $\sigma = 3$; diamonds, $\sigma = 6$. The lines are to guide the eye. Statistical errors are approximately the same size as the plotting symbols.

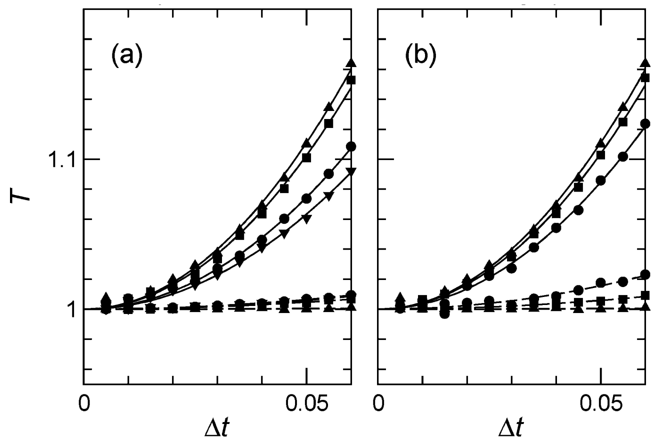

Figure 2. Water simulations using (a) a Stoyanov−Groot thermostat and (b) a Lowe thermostat: temperatures as functions of time step Δt; solid lines, configurational temperature T_c; dashed lines, kinetic temperature T_k; downward triangles, $\Gamma = 0$; circles, $\Gamma = 0.5$; squares, $\Gamma = 4$; upward triangles, $\Gamma = 1/\Delta t$ (maximum possible). The lines are to guide the eye. Statistical errors are approximately the same size as the plotting symbols.

$\Gamma = 0.5$ (i.e., $P = 0.025$ at $\Delta t = 0.05$), the Stoyanov−Groot method becomes similar in performance to the other methods.

For the membrane simulations, temperatures for each of the bead types (species) are reported in Figures 3 and 4. There are several points of interest. First, the kinetic temperatures for different species are different, as already noted.[26] The discrepancies between T_k and T for the lipid beads are somewhat worse than those in the case of simple water at the same time steps, on the order of a few percent. The configurational temperatures are also different for the different species. For the lipid beads, they are all in *much* poorer agreement with the desired temperature, than for the water: at $\Delta t = 0.05$, T_c is too high by 80−90% for some of the tail beads. This indicates a serious departure from equilibrium. Second, numbering the tail beads T_1−T_6 with T_1 next to the head bead, the results for both T_k and T_c divide naturally into groups: {H,T_6}, {T_1,T_5}, {T_2,T_3,T_4}, and {W}. Within each group, the temperatures agree, almost to within the statistical error bars, and no attempt is made to distinguish them in the figures. This suggests[26] that the intramolecular stretching and bending potential terms (which are the same within each group) are the dominant factors in the

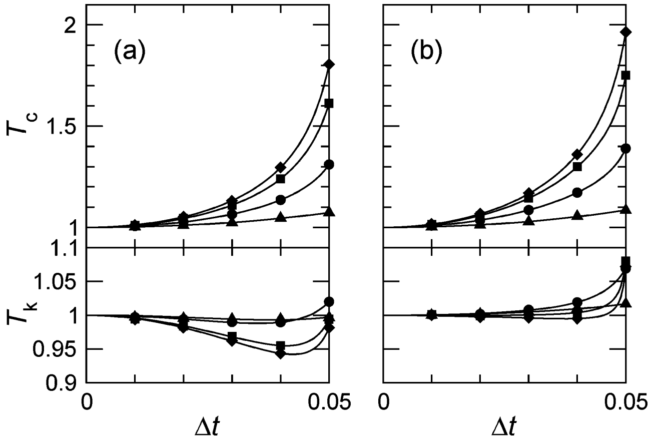

Figure 3. Membrane simulations using (a) a DPD algorithm with $\lambda = 0.65$ and $\sigma = 3.0$ and (b) Peters Scheme II with $\sigma = 3.0$: temperatures as functions of time step Δt; circles, H (head) and T_6 (tail) beads; squares, T_1 and T_5 beads; diamonds, T_2, T_3, and T_4 beads; triangles, W (water) beads. The lines are to guide the eye. Statistical errors are approximately the same size as the plotting symbols.

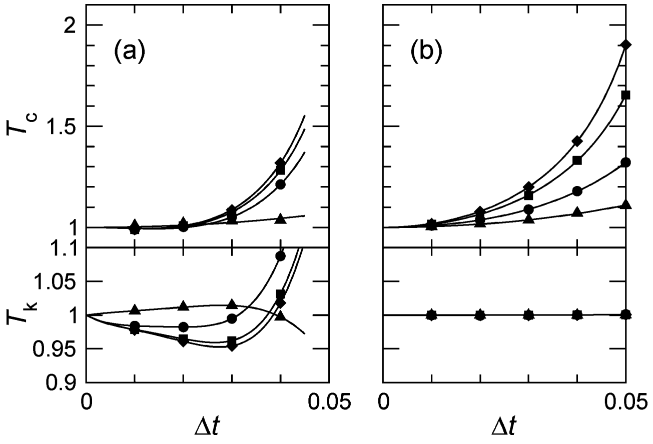

Figure 4. Membrane simulations using (a) a Stoyanov−Groot thermostat with $\Gamma = 0$ and (b) a Lowe thermostat with $\Gamma = 1/\Delta t$. Temperatures as functions of time step Δt. Symbols as for Figure 3.

problems of maintaining equilibrium; in the following section, some support will be given to this view, but it is also argued that the intermolecular potentials make a contribution. Of the four algorithms studied, the DPD, Peters, and heavily thermostatted Lowe method perform in a similar way to each other. The behavior of the Stoyanov algorithm is unusual: although T_c is quite close to T up to $\Delta t = 0.03$, T_k shows an instability. As Δt increases, the water temperature falls dramatically below T, while the other species become much too hot. This effect makes the simulation unphysical for $\Delta t = 0.05$.

Density and temperature profiles are shown in Figure 5, selecting the Peters thermostat as being representative. Jakobsen et al.[26] report a time step dependence of the density profiles, specifically a change in the (small) concentrations of headgroup beads in the interior of the bilayer. The present simulations do not confirm such a systematic effect; however, the transverse dimensions of the system are much smaller than those of ref 26, so the relevant statistics and time scales may prevent resolution of the effect here. The temperature profiles are as expected from Figures 3 and 4, with the most dramatic indicators of lack of equilibrium in the regions occupied by tail beads {T_2,T_3,T_4}. A comparison of the different algorithms at fixed time step $\Delta t = 0.03$ is given in Figure 6. In the lipid tail region the Lowe thermostat (with the parameter Γ set to the maximum

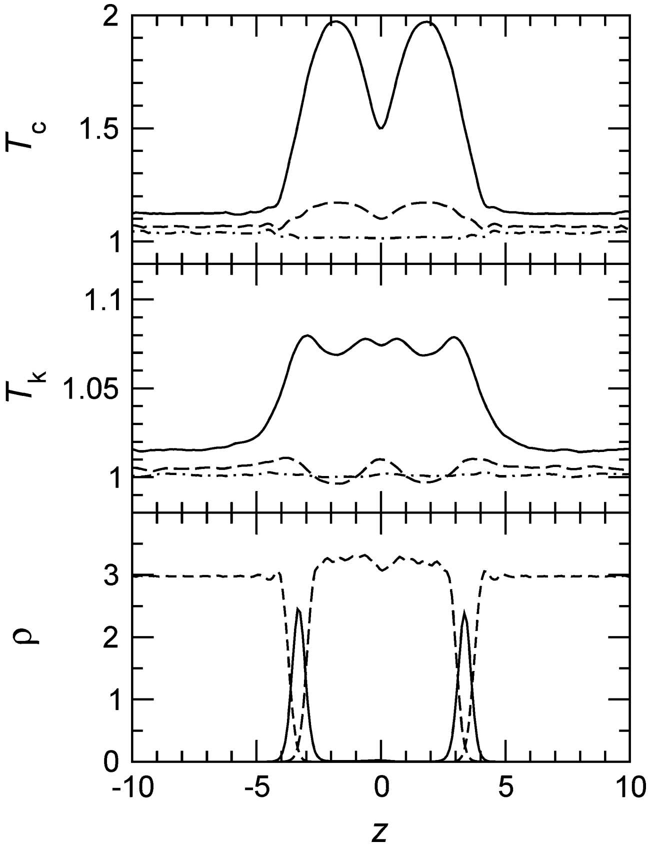

Figure 5. Density and temperature profiles in the bilayer region for membrane simulations using the Peters thermostat. The top two panels show configurational and kinetic temperatures as functions of time step: solid lines, $\Delta t = 0.05$; dashed lines, $\Delta t = 0.03$; dot−dashed lines, $\Delta t = 0.01$. Bottom panel shows, for reference, the local density, measured at $\Delta t = 0.01$: solid lines, H beads; long dashes, T beads; short dashes, W beads.

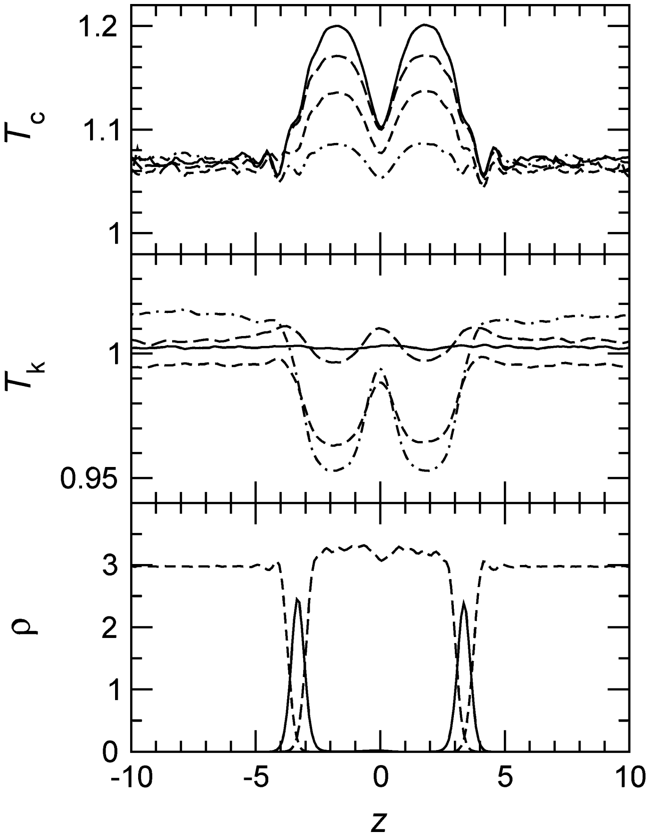

Figure 6. Density and temperature profiles in the bilayer region for membrane simulations at $\Delta t = 0.03$ using the different thermostats. The top two panels show configurational and kinetic temperatures: solid lines, Lowe thermostat with $\Gamma = 1/\Delta t$; long dashes, Peters thermostat with $\sigma = 3$; short dashes, DPD algorithm with $\sigma = 3$; dash−dotted line, Stoyanov−Groot thermostat with $\Gamma = 0$. Bottom panel shows, for reference, the local density, measured at $\Delta t = 0.01$: solid lines, H beads; long dashes, T beads; short dashes, W beads.

allowed value) gives the worst T_c, about 20% too high, while the Stoyanov thermostat (with $\Gamma = 0$) gives the best, about 8% too high; however the performance order is reversed for T_k with the Lowe thermostat (by construction) being perfectly accurate and the Stoyanov thermostat being overdamped by about 5%. The behavior in the water region does not give a good indicator of the lack of equilibrium within the membrane.

It is of interest to compare these profiles with the pressure tensor results which were also previously found to exhibit an anomaly.[26] The pressure profiles are calculated in the Irving−Kirkwood convention[31] using a method essentially the same as that described by Goetz and Lipowsky.[32] The results for the Peters thermostat are shown in Figure 7. The component P_N normal to the bilayer is not constant, contrary to what must hold for a system at equilibrium.[26] For $\Delta t = 0.05$ the error is comparable in magnitude to the physically interesting quantity, the difference $P_N - P_T$ between normal and transverse components, whose integral gives the surface tension. There is some cancellation of errors, since the anomaly appears in both components;[26] however, such an error is clearly undesirable. The point to be made here is that the configurational temperature profiles of Figure 5 are echoed in the pressure profiles of Figure 7.

5. Analysis and Discussion

It is evident that the configurational temperature gives a different perspective, from the kinetic temperature, on simulation equilibrium, even for simple fluids. Also the intramolecular bond stretching and bending potentials used in membrane simulations have a direct effect on the stability of the algorithm, which can be estimated via T_c, among other indicators.

Some insight into the information contained in T_c may be obtained by considering a very simple model: the one-dimensional harmonic oscillator, with Hamiltonian

$$\mathscr{H} = p^2/2m + \frac{1}{2}kx^2 \equiv K(p) + U(x)$$

It is known[33,34] that the velocity Verlet algorithm conserves *exactly* a “shadow Hamiltonian” which we may write in the form

$$\mathscr{H}^{\ddagger}(x,p) = p^2/2m + \frac{1}{2}kx^2(1 - \phi) \equiv K(p) + U^{\ddagger}(x)$$

where

$$\phi = \frac{1}{4}(k/m)\Delta t^2$$

A dynamical algorithm which alternates periods of velocity Verlet with velocity reselection from the canonical ensemble at temperature T (analogous to the “Lowe” algorithm of DPD) will actually generate momenta from the correct Maxwell−Boltzmann distribution $\exp(-\mathscr{H}/k_BT)$ and configurations from

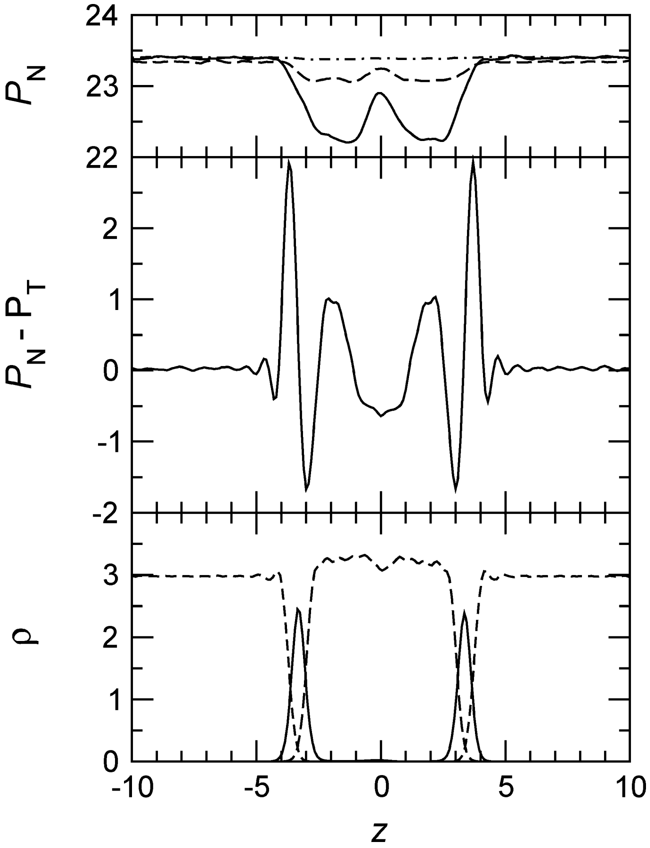

Figure 7. Density and pressure profiles in the bilayer region for membrane simulations using the Peters thermostat: (top panel) normal component P_N as a function of time step (solid lines) $\Delta t = 0.05$, (dashed lines) $\Delta t = 0.03$, (dot−dashed) lines) $\Delta t = 0.01$; (middle panel) surface tension integrand, $P_N - P_T$, measured at $\Delta t = 0.01$; (bottom panel) local density, measured at $\Delta t = 0.01$ (solid lines) H beads, (long dashes) T beads, (short dashes) W beads.

the “shadow distribution” $\exp(-\mathscr{U}^{\ddagger}/k_BT)$. An immediate consequence is

$$\frac{1}{2}k_BT = \langle p^2/2m\rangle = \left\langle\frac{1}{2}kx^2(1-\phi)\right\rangle$$

Since the force $f = -kx$ and $\partial^2\mathscr{H}/\partial x^2 = k$, the kinetic and configurational temperatures are

$$k_BT_k = \langle p^2/m\rangle = k_BT \tag{7a}$$

$$k_BT_c = \frac{\langle f^2\rangle}{\langle\partial^2\mathscr{H}/\partial x^2\rangle} = \frac{k_BT}{1-\phi} \tag{7b}$$

For a three-dimensional isotropic harmonic oscillator $U = 1/2\, k|\boldsymbol{r}|^2$, $\boldsymbol{f} = -k\boldsymbol{r}$ the same formula applies, with $k = {}^1/_3\nabla^2U$, and it is straightforward to extend it to the anisotropic case. The effect of an overly large time step is to reduce the effective force constant dictating the configurational distribution, increase the mean squared displacement, and (in proportion) increase the mean squared force which gives the value of T_c. The above equation is a reasonable first approximation to the curves shown in Figures 1 and 2. For the lipids, assuming that the intramolecular bond potentials are approximately harmonic, a given fractional error in T_c for each bead may approximately translate into a corresponding fractional error in mean-squared displacement which, when compounded along the chain, becomes a more significant error in overall flexibility.

TABLE 1: Laplacian ∇_i^2U for Beads in Lipid Chain Calculated for Isolated Chain at $T = 0$, as an Equilibrium Simulation Average at $T = 1$ for an Isolated Chain, from the Full Condensed Phase Simulation at $T = 1$, and from a Fit to the Measured T_c, Figure 8, Assuming a Locally Isotropic Harmonic Potential[a]

	single chain		condensed phase	
bead	$T = 0$	$T = 1$	$T = 1$	fit
H	288	273(2)	491(1)	1157(1)
T_1	1056	853(6)	1132(1)	1893(1)
T_2	1216	979(5)	1272(1)	2272(1)
T_3	1216	986(7)	1266(2)	2327(1)
T_4	1216	972(8)	1264(2)	2277(1)
T_5	1056	865(8)	1116(2)	1884(1)
T_6	288	267(3)	438(1)	1123(1)
W			122.8(1)	479(1)

[a] Figures in parentheses represent the estimated error in the last digit.

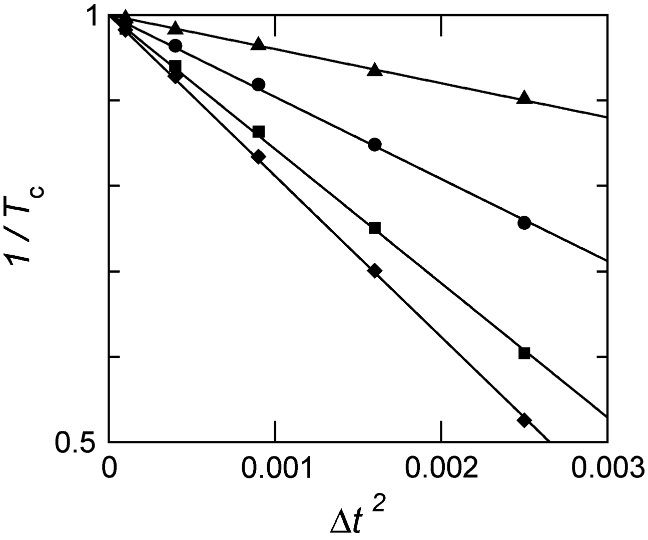

Figure 8. Membrane simulations using the Lowe thermostat with $\Gamma = 1/\Delta t$. Inverse configurational temperatures as functions of squared time step Δt^2. Symbols as for Figure 4b. Straight lines are fits using eq 7b.

It is tempting to try to estimate these contributions to T_c, for the isolated lipid chain. In the harmonic approximation, the appropriate force constants may be evaluated, taking the lipids to be in their minimum energy configuration and counting all the bonds in which a bead participates. In Table 1 the sum (over x, y, and z directions) of these predicted force constants (for $k_{\text{stretch}} = 128$, $l_0 = 0.5$, $k_{\text{bend}} = 20$) are compared with measured average Laplacians from simulations of a single chain at $T = 1$, and simulations of the full fluid system at $T = 1$, both conducted at short time steps.

The figures partly explain the close similarity in configurational temperatures within the groups of beads mentioned in the previous section, in terms of intramolecular potentials. There is some reduction in the average Laplacians due to fluctuations of the single chain at $T = 1$ compared with $T = 0$. However, in the full condensed phase simulation, this is more than compensated by an intermolecular contribution of order 200−250 in these reduced units, so part of this coincidence is due to the similar environments, and identical repulsion parameters between like beads, for this particular model.

The simulated fluids are not actually harmonic, and so the above analysis should not be overinterpreted. The Lowe thermostat results shown in Figure 4b are replotted in Figure 8 as T_c^{-1} vs Δt^2, for which eq 7b predicts a linear relationship.

The straight line fits are excellent, but the fitted parameters, presented in the final column of Table 1, are all significantly larger than would have been expected. Partly, this can be explained by the anisotropy of the local harmonic potential: the stiffest potentials will dominate the breakdown of the algorithm. However one should also remember that the real shadow Hamiltonian is more complicated than a simple harmonic potential and will not split in the same way into a kinetic part plus a renormalized configurational part.

Some effort has been made to develop practical methods to estimate the shadow Hamiltonian for complex systems.[35,36] Knowledge of this function may help not only the monitoring of algorithm performance but also the implementation of more efficient algorithms such as hybrid Monte Carlo.[37] This method differs from DPD in the rejection of moves so as to guarantee that the desired ensemble is sampled. Returning to the points made by Hafskjold et al.,[27] it is notable that *smoothness* of the potential is a highly desirable feature in the accurate construction of shadow Hamiltonians. To illustrate this, Engle et al.[36] considered a simple harmonic oscillator potential, modified by splitting into two halves at the minimum, with a flat piece inserted between them. The consequent lack of smoothness was shown to degrade conservation of the shadow Hamiltonian. Such a potential is a possible one-dimensional model system for the numerical aspects of DPD dynamics: the oscillation back and forth represents the motion of a DPD bead out of the repulsive quadratic potential of a neighbor and into the repulsive range of a different neighbor. In the absence of an improved algorithm to handle the DPD conservative forces, using a shorter time step for them seems the best approach.[17]

6. Conclusions

The essential conclusion of this paper is that stiffer potentials, and stronger conservative forces, require shorter time steps. This is hardly a new point and is increasingly being recognized in the DPD community,[17,27,26] where the principal danger is that the effects of an overly long time step may be disguised by the thermostat. It is recommended here that the configurational temperature T_c be measured and reported in DPD simulations, along with other indicators that the system is not at equilibrium, so as to address this danger. T_c is easy to calculate, and appears to be sensitive to some of the artifacts that appear in other properties such as the pressure tensor profile in membranes.

The degree of accuracy of sampling required will, no doubt, vary from one application to another. For the standard water model, Groot and Warren[3] recommended time steps $\Delta t \approx 0.05$, so as to achieve an accuracy of order 1% in T_k. Applying the same criterion to T_c would lead to a revised recommendation, $\Delta t \approx 0.015$. Modern thermostats are dramatically better at controlling T_k and give modest improvements in T_c. Stoyanov and Groot[18] note, for instance, that their new method keeps T_k within the desired 1% range even for $\Delta t = 0.09$; however, such a time step would result in an error in T_c between 24% and 44% depending on Γ. Also, for multicomponent systems such as lipid membranes, there may be substantial imbalances in the distribution of T_k and T_c between the different species. Such large discrepancies indicate lack of equilibrium; i.e., configurations are being sampled incorrectly.

It would, no doubt, be possible to devise thermostats that control the value of T_c as well as T_k and that act separately on the different types of bead. In such a case, it becomes important to measure other, independent, quantities as a function of time step and to bear in mind that no single quantity acts as an indicator of equilibrium.

Acknowledgment. The simulations reported here were performed on the computing facilities of the Centre for Scientific Computing, University of Warwick. Funding was provided by EPSRC Materials Modeling Initiative Grant GR/S80127. The referee is thanked for the suggestion to include Figure 8.

Appendix

The calculation of the Laplacian for each of the potential terms used in this study proceeds as follows. The DPD repulsive potential between i and j, with $\boldsymbol{r}_{ij} = \boldsymbol{r}_i - \boldsymbol{r}_j$, takes the form (assuming $r_{ij} \le r_c$)

$$u = \frac{1}{2}\left(\frac{\alpha}{r_c}\right)(r_{ij} - r_c)^2$$

The gradients (the negatives of which are the conservative forces of eq 3) are

$$\nabla_i u = -\nabla_j u = \alpha\left(\frac{r_{ij}}{r_c} - 1\right)\hat{\boldsymbol{r}}_{ij}$$

and the Laplacians are

$$\nabla_i^{2} u = \nabla_j^{2} u = \alpha\left(\frac{3}{r_c} - \frac{2}{r_{ij}}\right)$$

The formulas for the bond stretching potential of eq 6a are identical, with the replacements $r_c \rightarrow l_0$ and $\alpha \rightarrow k_{\text{stretch}} l_0$.

For the angle-bending potential of eq 11 between successive beads i, j, k, define $c_{ij} = \boldsymbol{r}_{ij}\cdot\boldsymbol{r}_{ij}$, $c_{jk} = \boldsymbol{r}_{jk}\cdot\boldsymbol{r}_{jk}$, $c_{ijk} = \boldsymbol{r}_{ij}\cdot\boldsymbol{r}_{jk}$. The gradients of these scalar products with respect to individual positions are

$$\begin{bmatrix} \nabla_i c_{ij} = 2\boldsymbol{r}_{ij} & \nabla_i c_{jk} = 0 & \nabla_i c_{ijk} = \boldsymbol{r}_{jk} \\ \nabla_j c_{ij} = -2\boldsymbol{r}_{ij} & \nabla_j c_{jk} = 2\boldsymbol{r}_{jk} & \nabla_j c_{ijk} = \boldsymbol{r}_{ij} - \boldsymbol{r}_{jk} \\ \nabla_k c_{ij} = 0 & \nabla_k c_{jk} = -2\boldsymbol{r}_{jk} & \nabla_k c_{ijk} = -\boldsymbol{r}_{ij} \end{bmatrix}$$

The Laplacians are

$$\begin{bmatrix} \nabla_i^{2} c_{ij} = 6 & \nabla_i^{2} c_{jk} = 0 & \nabla_i^{2} c_{ijk} = 0 \\ \nabla_j^{2} c_{ij} = 6 & \nabla_j^{2} c_{jk} = 6 & \nabla_j^{2} c_{ijk} = -6 \\ \nabla_k^{2} c_{ij} = 0 & \nabla_k^{2} c_{jk} = 6 & \nabla_k^{2} c_{ijk} = 0 \end{bmatrix}$$

The potential has the form $u_{\text{bend}} = k_{\text{bend}}(1 - C)$, where

$$C = \cos\theta_{ijk} = c_{ij}^{-1/2}\, c_{jk}^{-1/2}\, c_{ijk}$$

The necessary gradients are

$$\nabla_i C = (\nabla_i c_{ij}^{-1/2}) c_{jk}^{-1/2} c_{ijk} + c_{ij}^{-1/2}(\nabla_i c_{jk}^{-1/2}) c_{ijk} + c_{ij}^{-1/2} c_{jk}^{-1/2}(\nabla_i c_{ijk})$$

$$= c_{ij}^{-1/2} c_{jk}^{-1/2}\left(\boldsymbol{r}_{jk} - \frac{c_{ijk}}{c_{ij}}\boldsymbol{r}_{ij}\right)$$

$$\nabla_j C = (\nabla_j c_{ij}^{-1/2}) c_{jk}^{-1/2} c_{ijk} + c_{ij}^{-1/2}(\nabla_j c_{jk}^{-1/2}) c_{ijk} + c_{ij}^{-1/2} c_{jk}^{-1/2}(\nabla_j c_{ijk})$$

$$= c_{ij}^{-1/2} c_{jk}^{-1/2}\left(\left(1 + \frac{c_{ijk}}{c_{ij}}\right)\boldsymbol{r}_{ij} - \left(1 + \frac{c_{ijk}}{c_{jk}}\right)\boldsymbol{r}_{jk}\right)$$

$$
\begin{aligned}
\nabla_k C &= (\nabla_k c_{ij}^{-1/2}) c_{jk}^{-1/2} c_{ijk} + c_{ij}^{-1/2} (\nabla_k c_{jk}^{-1/2}) c_{ijk} + c_{ij}^{-1/2} c_{jk}^{-1/2} (\nabla_k c_{ijk}) \\
&= c_{ij}^{-1/2} c_{jk}^{-1/2} \left(\frac{c_{ijk}}{c_{jk}} \boldsymbol{r}_{jk} - \boldsymbol{r}_{ij} \right)
\end{aligned}
$$

The Laplacians are given by

$$
\begin{aligned}
\nabla_i^2 C &= (\nabla_i^2 c_{ij}^{-1/2}) c_{jk}^{-1/2} c_{ijk} + c_{ij}^{-1/2} (\nabla_i^2 c_{jk}^{-1/2}) c_{ijk} + c_{ij}^{-1/2} c_{jk}^{-1/2} (\nabla_i^2 c_{ijk}) + 2 c_{ij}^{-1/2} (\nabla_i c_{jk}^{-1/2} \cdot \nabla_i c_{ijk}) + \\
&\quad 2 c_{jk}^{-1/2} (\nabla_i c_{ijk} \cdot \nabla_i c_{ij}^{-1/2}) + 2 c_{ijk} (\nabla_i c_{ij}^{-1/2} \cdot \nabla_i c_{jk}^{-1/2}) \\
&= -2 c_{ij}^{-3/2} c_{jk}^{-1/2} c_{ijk}
\end{aligned}
$$

$$
\begin{aligned}
\nabla_j^2 C &= (\nabla_j^2 c_{ij}^{-1/2}) c_{jk}^{-1/2} c_{ijk} + c_{ij}^{-1/2} (\nabla_j^2 c_{jk}^{-1/2}) c_{ijk} + c_{ij}^{-1/2} c_{jk}^{-1/2} (\nabla_j^2 c_{ijk}) + 2 c_{ij}^{-1/2} (\nabla_j c_{jk}^{-1/2} \cdot \nabla_j c_{ijk}) + \\
&\quad 2 c_{jk}^{-1/2} (\nabla_j c_{ijk} \cdot \nabla_j c_{ij}^{-1/2}) + 2 c_{ijk} (\nabla_j c_{ij}^{-1/2} \cdot \nabla_j c_{jk}^{-1/2}) \\
&= -2 c_{ij}^{-3/2} c_{jk}^{-3/2} (c_{ijk}^2 + c_{ijk}(c_{ij} + c_{jk}) + c_{ij} c_{jk})
\end{aligned}
$$

$$
\begin{aligned}
\nabla_k^2 C &= (\nabla_k^2 c_{ij}^{-1/2}) c_{jk}^{-1/2} c_{ijk} + c_{ij}^{-1/2} (\nabla_k^2 c_{jk}^{-1/2}) c_{ijk} + c_{ij}^{-1/2} c_{jk}^{-1/2} (\nabla_k^2 c_{ijk}) + 2 c_{ij}^{-1/2} (\nabla_k c_{jk}^{-1/2} \cdot \nabla_k c_{ijk}) + \\
&\quad 2 c_{jk}^{-1/2} (\nabla_k c_{ijk} \cdot \nabla_k c_{ij}^{-1/2}) + 2 c_{ijk} (\nabla_k c_{ij}^{-1/2} \cdot \nabla_k c_{jk}^{-1/2}) \\
&= -2 c_{ij}^{-1/2} c_{jk}^{-3/2} c_{ijk}
\end{aligned}
$$

All of the above results should be multiplied by $(-k_{\mathrm{bend}})$ to give the gradients and Laplacians for the bending potential of eq 6b.

It is worth emphasizing that the dissipative and random terms in the DPD equations (2) play no role in the calculation of Laplacians and squared forces which go into the configurational temperature, eq 1.

References and Notes

(1) Hoogerbrugge, P. J.; Koelman, J. M. V. A. *Europhys. Lett.* **1992**, *19*, 155−160.

(2) Koelman, J. M. V. A.; Hoogerbrugge, P. J. *Europhys. Lett.* **1993**, *21*, 363−368.

(3) Groot, R. D.; Warren, P. B. *J. Chem. Phys.* **1997**, *107*, 4423−4435.

(4) Groot, R. D.; Rabone, K. L. *Biophys. J.* **2001**, *81*, 725−736.

(5) Kranenburg, M.; Venturoli, M.; Smit, B. *Phys. Rev. E* **2003**, *67*, 060901.

(6) Shillcock, J. C.; Lipowsky, R. *J. Chem. Phys.* **2002**, *117*, 5048−5061.

(7) Kranenburg, M.; Smit, B. *FEBS Lett.* **2004**, *568*, 15−18.

(8) Venturoli, M.; Smit, B.; Sperotto, M. M. *Biophys. J.* **2005**, *88*, 1778−1798.

(9) Pagonabarraga, I.; Hagen, M. H. J.; Frenkel, D. *Europhys. Lett.* **1998**, *42*, 377−382.

(10) Lowe, C. P. *Europhys. Lett.* **1999**, *47*, 145−151.

(11) Gibson, J. B.; Chen, K. *Int. J. Mod. Phys. C* **1999**, *10*, 241−261.

(12) Besold, G.; Vattulainen, I.; Karttunen, M.; Polson, J. M. *Phys. Rev. E* **2000**, *62*, R7611−R7614.

(13) Den Otter, W. K.; Clarke, J. H. R. *Europhys. Lett.* **2001**, *53*, 426−431.

(14) Vattulainen, I.; Karttunen, M.; Besold, G.; Polson, J. M. *J. Chem. Phys.* **2002**, *116*, 3967−3979.

(15) Nikunen, P.; Karttunen, M.; Vattulainen, I. *Comput. Phys. Commun.* **2003**, *153*, 407−423.

(16) Shardlow, T. *SIAM J. Sci. Comput.* **2003**, *24*, 1267−1282.

(17) Peters, E. A. J. F. *Europhys. Lett.* **2004**, *66*, 311−317.

(18) Stoyanov, S. D.; Groot, R. D. *J. Chem. Phys.* **2005**, *122*, 114112.

(19) Espanol, P.; Warren, P. *Europhys. Lett.* **1995**, *30*, 191−196.

(20) Marsh, C. A.; Yeomans, J. M. *Europhys. Lett.* **1997**, *37*, 511−516.

(21) Den Otter, W. K.; Clarke, J. H. R. *Int. J. Mod. Phys. C* **2000**, *11*, 1179−1193.

(22) Hirschfelder, J. O. *J. Chem. Phys.* **1960**, *33*, 1462−1466.

(23) Powles, J. G.; Rickayzen, G.; Heyes, D. M. *Mol. Phys.* **2005**, *103*, 1361−1373.

(24) Rugh, H. H. *Phys. Rev. Lett.* **1997**, *78*, 772−774.

(25) Butler, B. D.; Ayton, G.; Jepps, O. G.; Evans, D. J. *J. Chem. Phys.* **1998**, *109*, 6519−6522.

(26) Jakobsen, A. F.; Mouritsen, O. G.; Besold, G. *J. Chem. Phys.* **2005**, *122*, 204901.

(27) Hafskjold, B.; Liew, C. C.; Shinoda, W. *Mol. Simul.* **2004**, *30*, 879−885.

(28) Nosé, S. *Mol. Phys.* **1984**, *52*, 255−268.

(29) Hoover, W. G. *Phys. Rev. A* **1985**, *31*, 1695−1697.

(30) Berendsen, H. J. C.; Postma, J. P. M.; van Gunsteren, W. F.; DiNola, A.; Haak, J. R. *J. Chem. Phys.* **1984**, *81*, 3684−3690.

(31) Schofield, P.; Henderson, J. R. *Proc. R. Soc. London, Ser. A* **1982**, *379*, 231−246.

(32) Goetz, R.; Lipowsky, R. *J. Chem. Phys.* **1998**, *108*, 7397−7409.

(33) Toxvaerd, S. *Phys. Rev. E* **1994**, *50*, 2271−2274.

(34) Gans, J.; Shalloway, D. *Phys. Rev. E* **2000**, *61*, 4587−4592.

(35) Skeel, R. D.; Hardy, D. J. *SIAM J. Sci. Comput.* **2001**, *23*, 1172−1188.

(36) Engle, R. D.; Skeel, R. D.; Drees, M. *J. Comput. Phys.* **2005**, *206*, 432−452.

(37) Izaguirre, J. A.; Hampton, S. S. *J. Comput. Phys.* **2004**, *200*, 581−604.